biomass

MDPI

Article

Response-Surface-Based Optimization of Pyrolysis Parameters for Enhanced Fixed-Carbon Content and High Heating Value of Pili (*Canarium ovatum* Engl.) Nutshell-Derived Biochar

Arly Morico [1,2], Jeffrey Lavarias [1,2], Wendy Mateo [1,*], Antonio Barroga [3], Melba Denson [1], Kaye Papa [1], Marvin Valentin [2,4] and Andrzej Białowiec [2]

[1] Department of Agricultural and Biosystems Engineering, College of Engineering, Central Luzon State University, Science City of Muñoz 3120, Nueva Ecija, Philippines; morico.arly@clsu2.edu.ph (A.M.); jeffreylavarias@clsu.edu.ph (J.L.); mddenson@clsu.edu.ph (M.D.); kaye.papa@clsu2.edu.ph (K.P.)
[2] Department of Applied Bioeconomy, Wrocław University of Environmental and Life Sciences, 37a Chełmońskiego Str., 51-630 Wrocław, Poland; marvin.valentin@upwr.edu.pl (M.V.); andrzej.bialowiec@upwr.edu.pl (A.B.)
[3] Department of Animal Science, College of Agriculture, Central Luzon State University, Science City of Muñoz 3120, Nueva Ecija, Philippines; ajbarroga@clsu.edu.ph
[4] Department of Agricultural and Biosystems Engineering, College of Engineering, Benguet State University, Km. 5, La Trinidad 2601, Benguet, Philippines
* Correspondence: wcmateo@clsu.edu.ph

Abstract

Waste is increasingly recognized as misplaced biomass, underscoring its potential for reintegration into sustainable environmental management strategies. Biomass pyrolysis has emerged as a promising value-adding process capable of enhancing material properties for diverse applications. In this study, discarded Pili (*Canarium ovatum* Engl.) nutshells (PS) were utilized as a pyrolysis feedstock to upgrade their fuel characteristics. Pyrolysis conditions were optimized using response surface methodology (RSM) based on a central composite design (CCD) to maximize fixed-carbon content and higher heating value (HHV). The optimized biochar achieved a maximum fixed-carbon content of 86.15% and an HHV of 32.10 MJ/kg at a pyrolysis temperature of 600 °C and a residence time of 60 min, values comparable to those of conventional coal. Under these optimized conditions, the fixed-carbon content and HHV of the precursor biomass were enhanced by up to 254.7% and 58.4%, respectively. Statistical analysis indicated that pyrolysis temperature was the most significant factor influencing both fixed-carbon content and HHV ($p < 0.05$). The optimized biochar exhibited low volatile matter (8.88%), low ash content (4.97%), and low atomic ratios (H:C = 0.291; O:C = 0.077), indicating a high degree of carbonization and thermal stability. Energy-dispersive X-ray (EDX) analysis identified alkali and alkaline earth metals (Ca, Mg, Na), which contributed to the ash fraction, with minor heavy metals present, predominantly Pb. Hence, these findings enhance understanding of how pyrolysis conditions affect PS–biochar properties, improving fuel quality indicators.

Keywords: pili nutshell; pyrolysis; optimization; RSM; solid fuel; biochar; fixed carbon; high heating value

Check for updates

Academic Editor: Kaveh Khalilpour

Received: 31 December 2025
Revised: 6 February 2026
Accepted: 23 February 2026
Published: 5 March 2026

Copyright: © 2026 by the authors. Licensee MDPI, Basel, Switzerland. This article is an open access article distributed under the terms and conditions of the Creative Commons Attribution (CC BY) license.

1. Introduction

Canarium ovatum Engl., locally known as pili, is a tropical nut-bearing tree belonging to the *Burseraceae* family and the *Canarium* L. genus, which includes 75 tropical and subtropical species found in Asia, Africa, and the Pacific [1]. The species is endemic to the

Philippines and is a regionally significant tree in the Bicol region, recognized as its center of genetic diversity. Pili nut, which is the main product of the tree, has high economic value, particularly due to the quality of its oil, making it a promising export commodity [2,3]. From 2020 to 2022, the Philippines produced an average of 5.98 thousand metric tons of pili nuts annually, with exports averaging approximately 27 metric tons per year [4]. Structurally, the pili nut consists of pulp (68%), shell (25%), and kernel (7%) [5]. Pili nut is a nutritionally valuable fruit rich in essential minerals, with K and Ca dominant in the pulp and K, P, and Mg prevalent in the kernel, along with trace elements such as Fe, Zn, Mn, and Cu. The minerals in both pulp and kernel exhibit high bioavailability, particularly Mg and Ca [6], and the pulp oil and leaf extracts have been reported to possess antioxidant and antibacterial properties [7,8]. However, during processing, the hard pili nutshell (PS) is often discarded as waste despite its high lignocellulosic content and favorable characteristics for thermochemical conversion.

In the drive toward sustainability, bio-circular economy redefines waste as a misplaced resource, emphasizing its potential for reintegration into environmental management. Biochar, a carbon-rich material produced via pyrolysis at 350–1000 °C under low-oxygen conditions [9], has the potential to mitigate cumulative emissions of 66–130 billion metric tons of CO_2 equivalent over a century [10]. Its physicochemical properties, including specific surface area, porosity, cation exchange capacity, oxygen-containing functional groups, and mineral content, make it useful for addressing environmental challenges such as climate change [11], soil degradation [12], and pollution control [13].

However, biochar properties are strongly influenced by feedstock characteristics and pyrolysis conditions, such as temperature and residence time. Increasing pyrolysis temperature generally leads to higher carbon content, increased specific surface area, and elevated pH, while decreasing hydrogen and oxygen content [14,15]. Biochar with higher carbon content and lower molar ratios (e.g., H:C and O:C) exhibits higher carbon stability and aromaticity [16,17]. Pyrolysis also drives the morphological transformation of inorganic compounds, including nutrients, alkali and alkaline earth metals (AAEMs), and heavy metals, which critically affect agronomic performance and environmental safety [18]. For example, Ca and Mg can ameliorate acidic soils and improve nutrient availability, while K enhances fertility in nutrient-depleted soils [19–21]. The release and bioavailability of heavy metals vary among feedstocks and depend on interactions with minerals and aromatic organic compounds at different temperatures [18], which needs to be further explored. Moreover, biochar with higher fixed-carbon content exhibits more efficient combustion and a higher heating value (HHV) than biochar with lower fixed carbon [22,23]. Fixed carbon is a key parameter to indicate fuel quality, as an increase in fixed carbon generally translates to a proportional increase in HHV, reflecting the greater amount of energy available during combustion. Through pyrolysis, the carbon content of biomass can be enriched, enhancing its thermal, i.e., fixed carbon and HHV, and combustion properties and resulting in biochar with improved fuel characteristics [23].

Optimizing pyrolysis parameters, such as temperature and residence time, is crucial for producing biochar with desired energy-related properties. Response surface methodology (RSM) enables statistically validated optimization with fewer experimental trials than full factorial designs, allowing the study of individual factors and their interactions while reducing experimental cost and variation [13,22,24].

Previous RSM-based studies have optimized biochar from various lignocellulosic feedstocks. For example, Pap et al. (2022) reported a 34.78% biochar mass yield and 71.9% fixed-carbon content for conifer brash biochar at 500 °C for 30 min in a muffle furnace [13]. Mohit (2023) found that optimized biochar achieved a biochar yield of 49.9%, fixed-carbon content of 68.7%, and HHV of 28.3 MJ/kg under microwave pyrolysis at

800 W for 8.6 min [22]. While these studies demonstrate the effectiveness of controlled pyrolysis for tailoring biochar properties, there is limited information on PS-derived biochar. In particular, the effect of pyrolysis parameters on fixed-carbon content and HHV of PS-derived biochar has not been systematically investigated.

Previous work on the characterization, kinetics, and thermodynamic analysis of PS found a high volatile matter, low ash content, and a high calorific value, suitable for bioenergy applications [25]. To date, no study has reported the preparation of PS-derived biochar using RSM optimization based on a central composite design (CCD). Therefore, this study aimed at optimizing pyrolysis conditions, specifically temperature and residence time, to produce biochar with enhanced fuel properties. At the same time, this study identified the optimal conditions for maximizing fixed-carbon content and HHV of PS-derived biochar. Furthermore, the physicochemical, morphological, inorganic (surface AAEMs and other metallic species), and thermal properties of biochar produced under optimized conditions were comprehensively evaluated.

2. Materials and Methods

2.1. Sample Preparation

The *Canarium ovatum* Engl. nutshells or PS (see Figure 1) used in this study were obtained from the Pili Processing Facility of the Albay Provincial Agricultural Office (APAO), Camalig, Albay, Philippines. To remove surface contaminants such as dust and soil, the samples were rinsed with distilled water and dried at 105 °C for 24 h in a laboratory oven (WHLL-125BE, ChemLand, Stargard, Poland), following the PN-EN ISO 18134-2:2017-03E standard [26]. The dried material was then ground using a biomass mill (LMN 400, TESTCHEM, Pszów, Poland) and sieved to ≤2 mm prior to pyrolysis experiments.

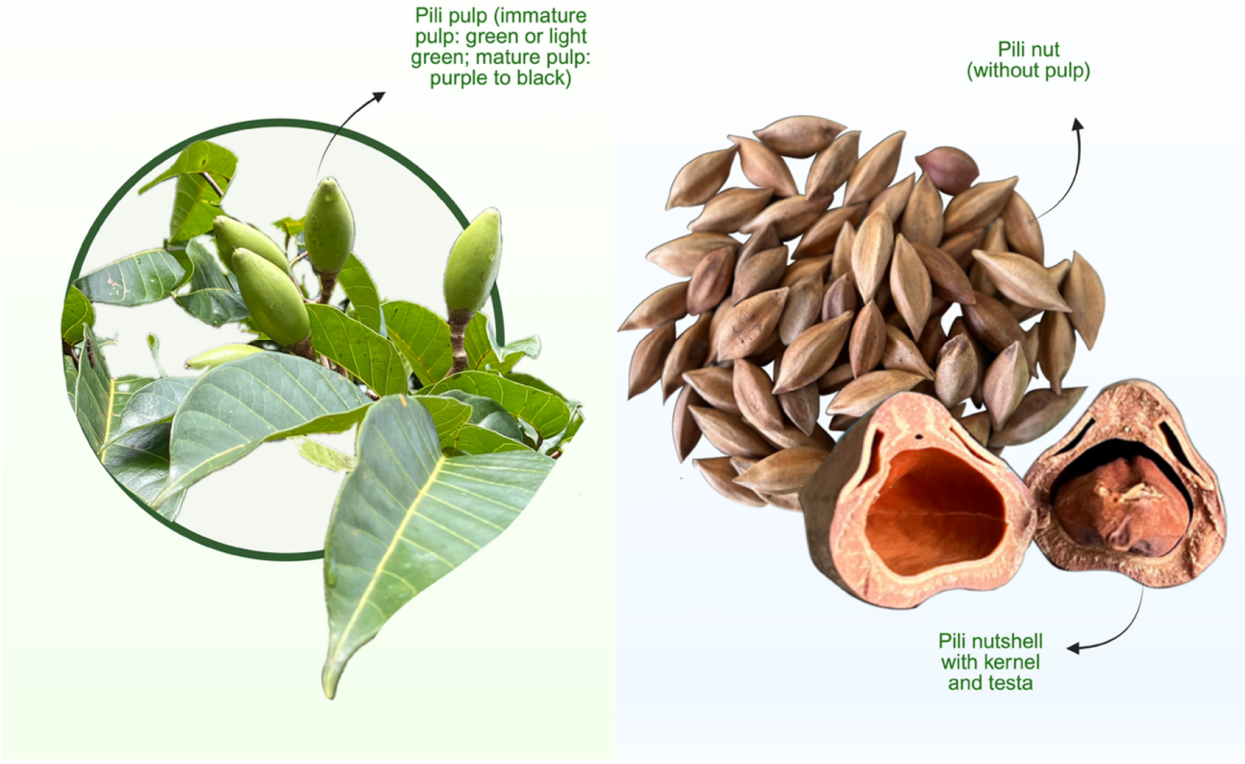

Figure 1. Pili fruit and pili shell obtained from Albay, Bicol, Philippines.

2.2. Experimental Setup and Design

Slow pyrolysis was carried out using a muffle furnace (Snol 8.1/1100, Utena, Lithuania). Approximately 50 g of biomass was placed in steel containers with base dimensions of 6 cm × 6 cm and a height of 8 cm. The containers were tightly closed to minimize oxygen ingress, with a small hole in the lid to allow evolved pyrolysis gases to escape [27]. Prior to heating, a CO_2 atmosphere was established by purging at 0.5 L/min for 30 min [28], while no additional CO_2 flow was applied during pyrolysis. The samples were then heated to the desired temperature for the specified residence time. After the pyrolysis process, the furnace was allowed to cool to room temperature. The resulting biochar was collected and stored in sealed plastic bags for further analysis. The biochar mass yield (MY) was calculated as the ratio of the biochar mass to the initial dry mass of the sample (Equation (1)). The energy densification ratio (EDr) and energy yield (EY) were subsequently determined using Equations (2) and (3) below [27,29]:

$$Mass\ yield\ (MY) = \frac{m_f}{m_i} \times 100 \quad (1)$$

$$Energy\ densification\ ratio\ (EDr) = \frac{HHV_f}{HHV_i} \times 100 \quad (2)$$

$$Energy\ yield\ (EY) = MY \times EDr \quad (3)$$

where m_i is the initial dry mass (g) of PS before pyrolysis, m_f is the final dry mass (g) of PS after pyrolysis, and HHV_i and HHV_f are the high heating value (MJ/kg) of PS before and after pyrolysis, respectively.

In the slow pyrolysis of PS, the RSM based on the CCD of the experiment was used to assess the effect of pyrolysis conditions such as temperature and residence time. These variables, representing energy input and the duration of pyrolysis, respectively, are among the most critical factors affecting pyrolysis performance [22]. Accordingly, in our previous work, the most significant weight loss on thermogravimetric analysis occurred at a temperature approaching 400 °C, with the rate of weight reduction slowing down to around 600 °C [25]. Based on these results, the temperature ranges of 400–600 °C were selected with a residence time varied within 60–120 min. The corresponding coded levels are presented in Table 1. A total of 13 experimental runs, including four factorial points, four axial points, and five center points, were designed using Design-Expert software (Trial version 13, Stat-Ease Inc., Minneapolis, MN, USA), as shown in Table 2. All experimental runs, including the five center-point runs at 500 °C and 90 min, were conducted as true independent pyrolysis experiments. The resulting HHV and fixed-carbon content were taken as the two response variables to be maximized. For each run, responses were measured twice to assess analytical repeatability. These responses were modeled using a polynomial as expressed in Equation (4):

$$Y = \beta_0 + \sum_{i=1}^{n} \beta_i X_i + \sum \beta_{ii} X_i^2 + \sum_{i=1}^{n-1} \sum_{j=i+1}^{n} \beta_{ij} X_i X_j + \in \quad (4)$$

where Y denotes the predicted response values, β_0 is constant, and β_i, β_{ii}, β_{ij} represent linear coefficient, quadratic coefficient, and interaction coefficients, respectively. X_i and X_j indicate the coded value of the independent variables, while $\in$ denotes the random error [13]. The polynomial model was analyzed using analysis of variance (ANOVA) to determine the statistical significance of the pyrolysis parameters at a 95% confidence level ($p < 0.05$). Model adequacy was assessed through the lack-of-fit test and the coefficient of determination (R^2). The 3D and contour response surface plots were generated to visualize the

interactions between variables and their effects on the responses. Numerical optimization was applied to identify the optimal pyrolysis conditions for maximizing the responses.

Table 1. Independent variables and their corresponding coded levels for the central composite design of experiments.

Independent Variables	Coded Factors					
	Units	$-\alpha$	−1	0	+1	$+\alpha$
Temperature (A)	°C	358.58	400	500	600	641.42
Residence time (B)	min	47.57	60	90	120	132.43

Table 2. Experimental design and results of the central composite design.

Experimental Run	Process Parameters		Response Variables			
			Fixed Carbon, %		HHV, MJ/kg	
	Temperature, °C	Time, Mins	Experimental	Predicted	Experimental	Predicted
1	600	60	86.15 ± 0.02	85.13	32.10 ± 0.06	32.30
2	500	90	67.30 ± 4.75	71.27	31.01 ± 0.01	31.00
3	500	47.57	73.82 ± 3.69	75.62	30.79 ± 0.06	30.60
4	600	120	85.30 ± 0.02	83.97	31.96 ± 0.02	31.88
5	500	132.43	77.90 ± 0.01	80.14	31.21 ± 0.03	31.41
6	500	90	69.44 ± 4.68	71.27	31.16 ± 0.02	31.00
7	641.42	90	86.50 ± 0.01	87.32	32.29 ± 0.01	32.54
8	500	90	68.49 ± 4.81	71.27	31.06 ± 0.06	31.00
9	500	90	73.40 ± 4.56	71.27	31.19 ± 0.04	31.00
10	358.58	90	65.30 ± 0.01	68.52	28.45 ± 0.04	29.46
11	400	120	78.06 ± 0.02	75.03	31.31 ± 0.11	30.69
12	500	90	77.73 ± 0.01	71.27	31.03 ± 0.03	31.00
13	400	60	70.20 ± 0.02	67.48	29.48 ± 0.01	29.14

2.3. Analytical Methods

A thermogravimetric analyzer (TGA/DSC 3+, Mettler Toledo, Greifensee, Switzerland) with a dynamic heating mode created in STAR^e software (version 16.40) was used to perform the proximate analysis of raw biomass and PS-derived biochar to identify moisture content, volatile matter, and ash content [30]. The fixed-carbon content was calculated by difference as given in Equation (5).

$$Fixed\ carbon\ (\%) = 100 - [MC\ (\%) + VM\ (\%) + AC\ (\%)] \quad (5)$$

The elemental compositions, which include carbon (C), hydrogen (H), nitrogen (N), and sulfur (S), were determined in duplicate using an elemental analyzer (PerkinElmer, 2400 CHNS/O Series II, Waltham, MA, USA), following the PN-EN ISO 16948:2015-07 standard [31]. Element oxygen (O) content was estimated by difference using Equation (6).

$$O = 100 - C\ (\%) - H\ (\%) - N\ (\%) - S\ (\%) - AC\ (\%) \quad (6)$$

The surface morphology and microscopic structure of the samples were characterized using a scanning electron microscope (SEM) (EVO LS 15, Oberkochen, Germany) at 16 kV electron high tension (EHT). Samples were gold-sputtered using a ScanCoat Six (Oxford Instruments, Abingdon, UK) to improve surface conductivity. Elemental composition and surface elemental mapping were analyzed using a BRUKER energy-dispersive

X-ray (EDX) system coupled to the SEM and operated at an accelerating voltage of 20 kV (Billerica, MA, USA).

The weight-change rate of the raw biomass and PS-derived biochar was measured using a thermogravimetric analyzer (TGA/DSC 3+, Mettler Toledo, Columbus, OH, USA). Approximately 5 mg of each sample was placed in an Al_2O_3 crucible (70 µL, Mettler Toledo) and analyzed under a pure nitrogen (N_2) atmosphere with a flow rate of 50 mL/min. The temperature ranged from 30 °C to 900 °C at a rate of 15 °C/min to simulate the heating conditions during the pyrolysis experiments. The pH of biochar was measured by employing a sample/deionized water ratio of 1:20 (w/v) after 24 h of mechanical shaking at 330 rpm (Biosan, PSU-10i, Riga, Latvia) under room temperature. Electrical conductivity was determined using a multifunction meter (Elmetron, model CX-705, Zabrze, Poland). The HHV was measured according to the PN-EN ISO 18125:2017-07 standard [32], using a bomb calorimeter (IKA, C200, Staufen, Germany). All tests were performed in duplicate.

3. Results and Discussion

3.1. Pili Nutshell Composition and Characteristics

Table 3 indicates the proximate, elemental, and compositional analysis for dried PS. PS exhibited a high volatile matter content of 73.93 ± 0.01%, with low moisture and ash content of 2.25 ± 0.01% and 1.78 ± 0.00%, respectively. These findings are favorable characteristics for thermochemical conversion processes such as pyrolysis [33,34]. Accordingly, volatile matter facilitates fuel ignition and affects flame stability [35]. However, fuels with higher volatile matter release less heat, as a large fraction of their mass is lost as volatiles.

Table 3. Physicochemical properties of pili nutshell.

Properties	Measured Values
Proximate analysis (wt%)	
Moisture content	2.25 ± 0.01
Volatile matter	73.93 ± 0.01
Ash content	1.78 ± 0.00
Fixed carbon	24.29 ± 0.01
Ultimate analysis (wt%) [1]	
Carbon	50.65 ± 0.60
Hydrogen	6.46 ± 0.04
Nitrogen	0.44 ± 0.08
Sulfur	1.16 ± 0.18
Oxygen	39.52 ± 0.47
H:C	1.53
O:C	0.59
Composition analysis (wt%) [1]	
Cellulose	33.84 ± 0.53
Hemicellulose	25.95 ± 0.53
Lignin	36.44 ± 2.21
Extractives	3.77 ± 0.08
HHV, MJ/kg	20.27 ± 0.01
pH	5.34 ± 0.01
Electrical conductivity, mS/cm	$0.15 \pm 8.6 \times 10^{-4}$

[1] values obtained from [25].

The share of C and O was 50.65 ± 0.60% and 39.52 ± 0.47%, respectively. These values are similar to those of *Canarium schweinfurthii* hard-shell [34]. The results showed that raw PS biomass has a molar ratio of O:C = 0.59 and H:C = 1.53. Additionally, a high sulfur content of 1.16 ± 0.18 wt% was observed in PS, which is higher than in typical agricultural waste residues [28].

Cellulose, hemicellulose, and lignin are the main structural components of biomass, each playing a distinct role during pyrolysis. Among them, lignin is the most thermally stable component and is primarily responsible for biochar formation due to its intricate aromatic structure [36]. High thermal stability of lignin contributes to increased biochar yield and fixed-carbon content relative to cellulose and hemicellulose [37]. PS with 33.84 ± 0.53% cellulose, 25.95 ± 0.53% hemicellulose, and 36.44 ± 2.21% lignin [25] falls within the typical ranges reported for nutshells [i.e., cellulose (25–35%), hemicellulose (25–30%), and lignin (30–40%) [38]. Moreover, PS exhibited a pH of 5.34 ± 0.01, a low electrical conductivity of 0.15 ± 8.6 × 10^{-4} mS/cm, and a HHV of 20.27 ± 0.01 MJ/kg, higher than that of many reported biofuel feedstocks [22,37].

3.2. Biochar Production Efficiency

A total of 13 experiments were designed using the CCD. The MY, EDr, and EY of PS-derived biochar under different pyrolysis conditions were summarized in Supplementary Table S1. MY ranged from 28.37 to 41.57%, and a higher yield was observed at lower pyrolysis temperature, particularly at 358.58 °C. At higher temperatures (600–641 °C), MY decreased and became less sensitive to residence time. For instance, at 600 °C, extending the residence time from 60 to 120 min caused a negligible change in MY (29.11% to 29.08%), indicating that most devolatilization occurred early in the process. At lower temperatures, residence time had a stronger effect at 400 °C. Increasing residence time from 60 to 120 min reduced MY from 37.38% to 31.55%, reflecting the progressive conversion of biomass into volatile compounds. This trend is consistent with the literature, which reported that prolonged heating leads to gradual biochar mass loss through secondary reactions such as gasification and thermal cracking [22].

The EDr ranged from 140.4 to 159.3%, with the highest values obtained at 641.42 °C, indicating enhanced carbonization and increased energy density at elevated temperatures. However, the increase in EDr with residence time was marginal. For instance, at 500 °C, increasing residence time from approximately 47.6 to 132.4 min increased EDr only slightly (151.9 to 154.0), while MY declined. Although biochar produced at higher temperatures is more energy-dense, the EY was moderated by reduced mass retention. Indeed, EY decreased at higher temperatures and longer residence times, reflecting severe conversion of biomass into liquid and gaseous products [39]. The highest EY (58.3%) was observed at 358.58 °C and 90 min, where higher MY compensated for lower EDr. These findings are consistent with previous reports [27], demonstrating that pyrolysis temperature dominates biochar yield and energy recovery, with residence time providing a secondary, temperature-dependent synergistic effect.

3.3. Model Development and Statistical Analysis Using Response Surface Methodology

The results of the experiments indicated 65.3–86.5% and 28.45–32.29 MJ/kg for fixed carbon and HHV, respectively (see Table 2). The highest fixed-carbon contents, corresponding to the highest HHV, were observed in experimental runs 1, 4, and 7. Consistent with the findings of a previous study [40], an increase in fixed carbon content was associated with a higher calorific value, indicating a strong positive correlation between fixed carbon and HHV in the studied coal.

3.3.1. Model Fitting and Regression Analysis for Fixed Carbon

The experimental response (Table 2) was modeled as a polynomial equation that represents the effect of experimental independent and dependent variables on the fixed carbon. Multiple regression analysis was applied to obtain the quadratic equation in terms of coded and actual factors, as given in Equations (7) and (8), respectively:

$$\textit{Fixed carbon}\ (\%) = +71.27 + 6.65(A) + 1.60(B) - 2.18\ (AB) + 3.33\ (A)^2 + 3.31(B)^2 \quad (7)$$

$$\textit{Fixed carbon}\ (\%) = +113.48467 - 0.2007978\ (\textit{temperature}) - 0.245008\ (\textit{time}) - 0.000726\ (\textit{temperature} \times \textit{time}) + 0.000333(\textit{temperature})^2 + 0.003673(\textit{time})^2 \quad (8)$$

Table 4 shows that the *F*-value of 6.61 and *p*-value of 0.0139 confirm the statistical significance of the model. Temperature (A) showed a significant linear effect ($F = 22.12$, $p < 0.05$) while its quadratic term (A^2) was marginally insignificant (*p*-values > 0.0642). In contrast, residence time (B) and its quadratic term (B^2), as well as the interaction term (AB), exhibited *p*-values greater than 0.05, indicating insignificant effects. Prolonged residence times at elevated temperatures may slightly reduce fixed-carbon content. This reduction is probably caused by the reintroduction of volatiles through repolymerization and recondensation reactions [22]. Conversely, secondary char formation from the gas phase necessitates particular conditions like high pressure. The fixed carbon yield stabilizes once the volatile matter in the feedstock has been released [15]. These mechanisms explain why residence time contributes negligibly to fixed carbon under the conditions investigated, and that maximal fixed-carbon content is primarily influenced by pyrolysis temperature.

Table 4. Analysis of variance for response variables model.

Terms	Fixed Carbon		High Heating Value	
	F-Value	*p*-Value Prob > F	F-Value	*p*-Value Prob > F
Model	6.61 *	0.0139	18.78 *	0.0003
A-Temperature	22.12 *	0.0022	48.08 **	<0.0001
B- Residence Time	1.28	0.2955	3.30	0.1025
AB	1.19	0.3120	4.94	0.0533
A^2	4.82	0.0642		
B^2	4.76	0.0655		
Lack of fit	0.7062 ^{ns}	0.5964	54.56 **	0.0009
Std. Deviation	4.00		0.4441	
Mean	75.35		31.00	
C.V.%	5.30		1.43	
R^2	0.8252		0.8622	
Adeq. Precision	7.3068		13.8323	

* significant at 0.05 level; ** significant at 0.01 level; ^{ns} not significant.

A non-significant lack of fit indicates that the model has good predictive capability. Since the *p*-value of the lack-of-fit test was greater than 0.05, the model fits the experimental data reasonably well [24]. The low CV reflects low dispersion and higher precision in predictions [41]. The observed CV of 5.30% suggests good model precision. The regression model showed an R^2 value of 0.8252. This implies that 82.52% of the sample variation can be explained by the model, and only 17.48% is outside the range that can be explained by the model. Although this R^2 value is lower than those reported for microalgae pyrolysis, it falls within the acceptable range (0.75–1.00) for a reliable predictive model [41]. Therefore, the developed quadratic model for PS pyrolysis can be considered statistically satisfactory. Accordingly, the acceptability of the model was based on the lowest standard deviation (SD) and the highest R^2 [42]. A low SD of 4.00 implies that the model's predictions are consistent [22]. Additionally, adequate precision values exceeding 4 confirm the models' predictive capability [41,43]. The adequate precision value of 7.31 indicates that the developed model is suitable for predicting fixed-carbon content.

3.3.2. Model Fitting and Regression Analysis for High Heating Value

In Table 2, the observed values for HHV were fitted to a polynomial model with two-factor interactions (2FI), and the corresponding statistical parameters were calculated.

The coded and actual relationships between HHV response and the test variables can be described by the following Equations (9) and (10), respectively.

$$HHV\ (\mathrm{MJ/kg}) = +31.00 + 1.09(A) + 0.2853(B) - 0.4936(AB) \quad (9)$$

$$HHV\ (\mathrm{MJ/kg}) = +17.29884 + 0.025697\ (temperature) + 0.091782\ (time) - 0.000165\ (temperature \times time) \quad (10)$$

The ANOVA for the HHV response (Table 4) indicates that the model is statistically significant ($p = 0.0003$). As shown in Table 3, temperature (A) is the most influential factor, with an F-value of 48.08 and a lower p-value of <0.0001. In contrast, residence time ($F = 3.30$, $p > 0.05$) and interaction between temperature and residence time (AB) ($p > 0.05$) are not statistically significant. During pyrolysis, most oxygen- and hydrogen-rich volatiles are released early, leaving a carbon-rich, energy-dense solid. Subsequent aromatization of carbon further increases energy density. Extended reaction times have minimal effect on HHV because the remaining carbon fraction is already stabilized, and only minor repolymerization or secondary reactions occur. Consequently, temperature is the only significant term affecting maximum HHV.

Model adequacy was further assessed using the lack-of-fit test and determination coefficients. The result indicates a statistically significant lack of fit ($F = 54.56$), suggesting that the selected 2FI model does not fully capture all systematic variability in the HHV response. This behavior may arise from unmodeled higher-order effects, local nonlinearities in the response surface, or experimental variability not adequately described by the current model structure [24,44]. Nevertheless, the relatively low SD of 0.4441 and CV of 1.43% indicate good experimental repeatability and analytical consistency. The R^2 of 0.8622 and an adequate precision value of 13.83 further suggest that the model provides a sufficient signal-to-noise ratio for exploratory analysis of the HHV response within the studied range. Consistent with this, across all temperatures, HHV shows minimal change with varying residence times, including center-point runs shows that the measured HHVs were relatively stable. The low variability in HHV supports the robustness of the model for identifying dominant factors and general response trends.

3.3.3. Diagnostic Plots

Diagnostic plots were used to assess the adequacy of the fitted models. For a good model, it is recommended that residuals be randomly and normally distributed [45]. As shown in Figure 2a,b, the predicted versus actual plots for fixed-carbon content and HHV, respectively, demonstrate good agreement, with most points lying close to the diagonal line. Figure 2c,d present the normal probability plots of externally studentized residuals for fixed-carbon content and HHV, respectively. Most points align closely with the diagonal line, with only a few points marginally outside, indicating that the models adequately capture the overall response trends [42]. For HHV (Figure 2d), one residual deviates slightly from the line, reflecting experimental variability. The plots of externally studentized residuals versus predicted values can be used to assess model adequacy and detect systematic errors [24]. For both fixed-carbon content and HHV (Figure 2e,f), most points are randomly distributed within acceptable limits, indicating no obvious trends and supporting model adequacy. For HHV (Figure 2f), one point slightly exceeds the diagnostic limits, suggesting a potential outlier or experimental variability [24]. Overall, the diagnostic plots confirm that the models are suitable for trend exploration and identification of dominant factors in the studied responses.

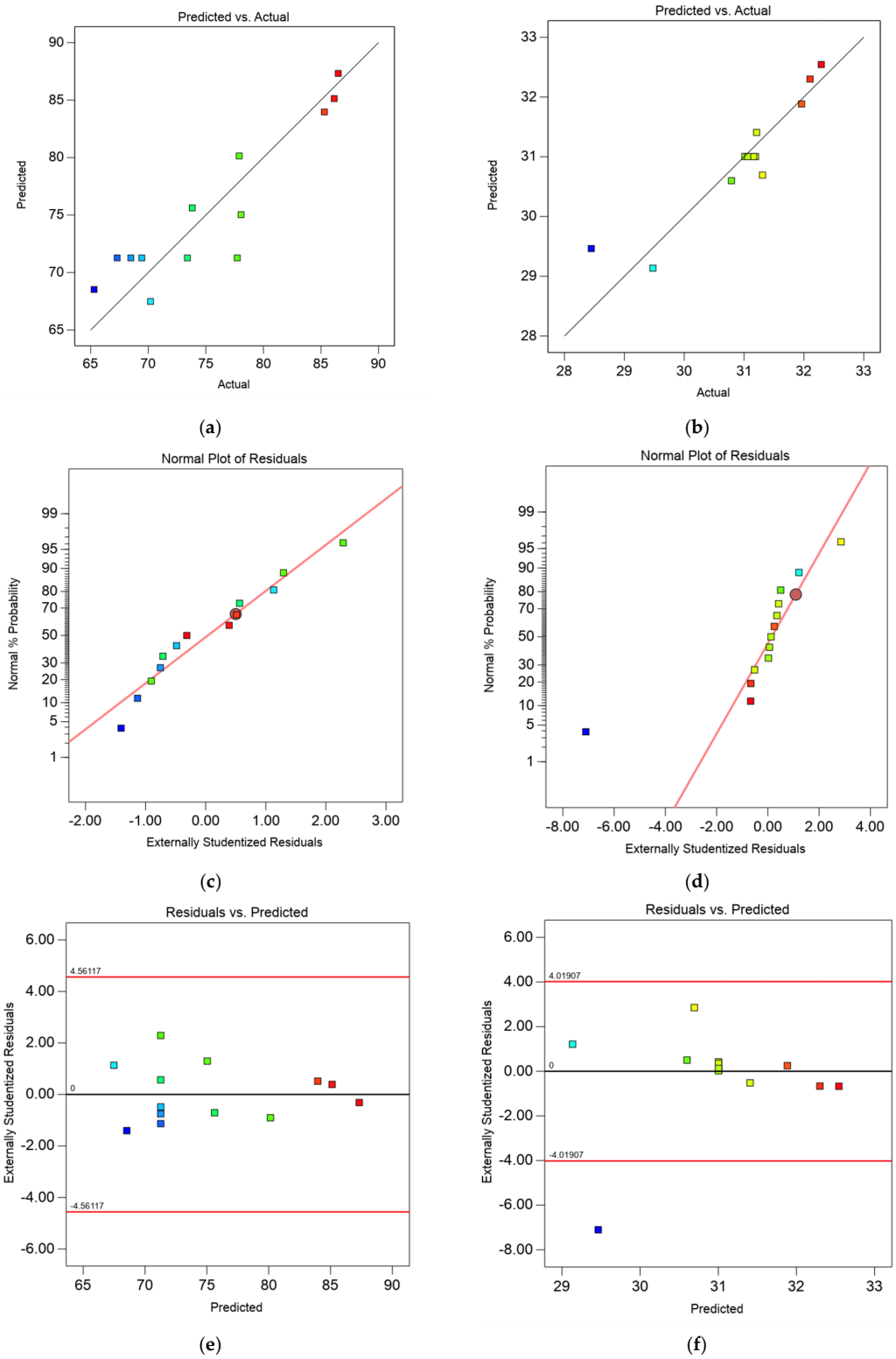

Figure 2. Predicted versus actual values plot for (**a**) fixed-carbon content and (**b**) HHV; and normal probability plot of residues for (**c**) fixed-carbon content and (**d**) HHV; Externally studentized residues versus predicted plot for (**e**) fixed-carbon content and (**f**) HHV.

3.4. Process Analysis

3.4.1. Effect of Process Parameters on Fixed Carbon

Figure 3a,b present the contour and 3D response surface plots. The figures illustrate the interactive effects of pyrolysis temperature and residence time on the fixed-carbon content of PS-derived biochar. The response surfaces indicate that pyrolysis temperature is

the primary controlling parameter, while the effect of residence time is dependent on temperature. At elevated temperatures (600–641 °C), fixed-carbon enrichment is maximized and shows minimal sensitivity to residence time. As summarized in Table 2, fixed-carbon contents ≥85 wt% were obtained at 600 °C for both 60 and 120 min (86.15 ± 0.02% and 85.30 ± 0.02%, respectively), while the highest fixed-carbon value (86.50 ± 0.01%) was achieved at 641.42 °C and 90 min. In contrast, at lower and intermediate temperatures, residence time exerts a more noticeable influence on fixed-carbon development, indicating incomplete devolatilization and ongoing secondary reactions. Similar temperature-dominated behavior has been reported for cassava peel biochar, where increasing pyrolysis temperature up to 600 °C significantly enhanced fixed carbon content (46.38–66.90 wt%) [23]. Temperatures above 600 °C promote secondary cracking reactions, leading to improved fixed-carbon quality through enhanced carbonization [46].

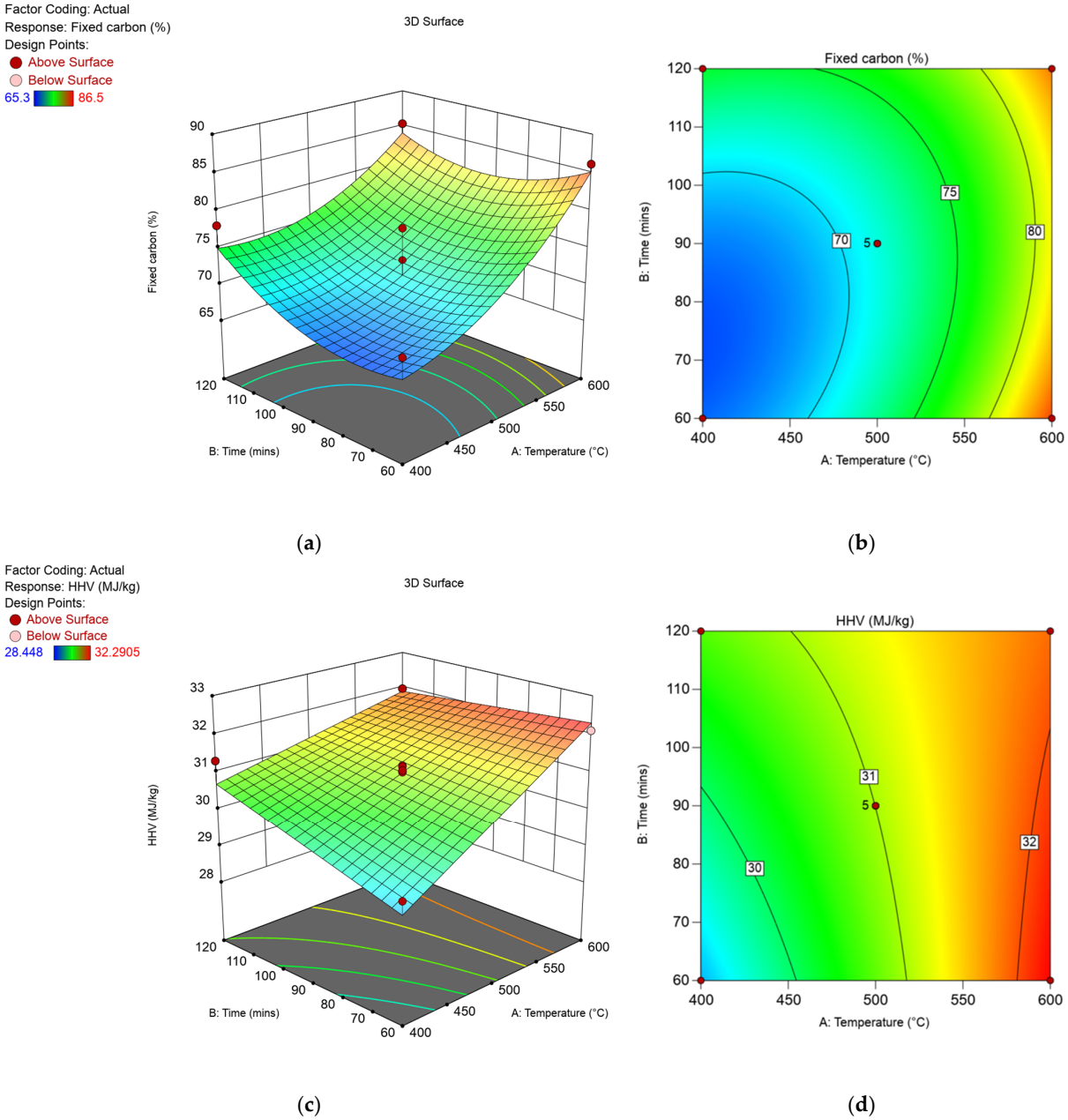

Figure 3. 3D and contour response surface plots on the effects of residence time and temperature on (**a**,**b**) fixed-carbon content and (**c**,**d**) HHV.

Mechanistically, higher pyrolysis temperatures accelerate volatile release and promote secondary carbonization, resulting in a carbon-enriched solid matrix [22,23,46]. Consequently, the interaction analysis confirms that temperature governs fixed-carbon formation, whereas residence time acts as a secondary parameter whose influence diminishes once major devolatilization reactions are completed. From a process-optimization standpoint, these results demonstrate that increasing temperature is more effective than extending residence time for maximizing fixed-carbon content within the studied operating window.

3.4.2. Effect of Process Parameters on High Heating Value

The effects of pyrolysis temperature and residence time on the HHV of PS-derived biochar are illustrated in Figure 3c,d. Experimentally measured HHV increased substantially with increasing pyrolysis temperature, whereas residence time exerted only a minor influence. The lowest HHV of 28.45 MJ/kg was recorded at 358.58 °C and 90 min, indicating incomplete devolatilization and limited carbonization at low temperature. In contrast, the maximum HHV of 32.29 MJ/kg was obtained at 641.42 °C and 90 min, while a comparable HHV of 32.10 MJ/kg was achieved at 600 °C and 60 min, demonstrating that high energy density can be attained even at shorter residence times once sufficiently high temperature is reached. Across the high-temperature region (600 °C), extending the residence time from 60 to 120 min resulted in only marginal changes in HHV ($\leq$0.14 MJ/kg), corresponding to less than 1% variation in energy content. This limited sensitivity explains the statistically insignificant effect of residence time and the negligible temperature–residence-time interaction observed in the results of ANOVA. The 3D response surface further confirms that HHV is primarily governed by pyrolysis temperature, while residence time plays a secondary role once thermal severity is sufficient. This is in contrast to the findings of a previous study [47], where a significant interaction effect between temperature and residence time was detected for the pyrolysis of rice straw.

Mechanistically, increasing pyrolysis temperature enhances devolatilization, aromatization, and secondary polymerization reactions, progressively enriching the carbon content of the biochar. This increase in C content results in greater mass–energy density, which consequently improves HHV [23]. Compared with other biomass feedstocks such as palm kernel shell [48], coconut shell [49], *Canarium schweinfurthii* shell [34], and walnut shell [50], the maximum HHV of PS-derived biochar was higher.

3.5. Numerical Optimization

Table 5 demonstrates the constraints present in each variable for numerical optimization of responses. The software suggests a total of 100 different solutions, and the solution with the highest desirability was considered optimum (Supplementary Table S2). The condition yielding the highest overall desirability corresponded to a pyrolysis temperature of 600 °C and a residence time of 60 min, with predicted values of 85.13% fixed carbon and 32.3 MJ/kg HHV (Figure 4). Importantly, these conditions coincided with one of the true independent experimental runs conducted during the RSM analysis, which results indicated 86.15% fixed carbon and 32.10 MJ/kg HHV, with MY of 29.11%, EDr of 158.4%, and EY of 46.1%. These results demonstrate that high-temperature, short-residence-time pyrolysis effectively produces biochar with concentrated energy content, balancing fuel quality and recoverable energy.

Table 5. Constraints of each variable for numerical optimization of responses.

Variable	Goal	Lower Limit	Upper Limit	Importance
A:Temperature	is in range	400	600	3
B:Time	is in range	60	120	3
Fixed carbon, %	maximize	65.3	86.15	3
HHV, MJ/kg	maximize	28.448	32.2905	3

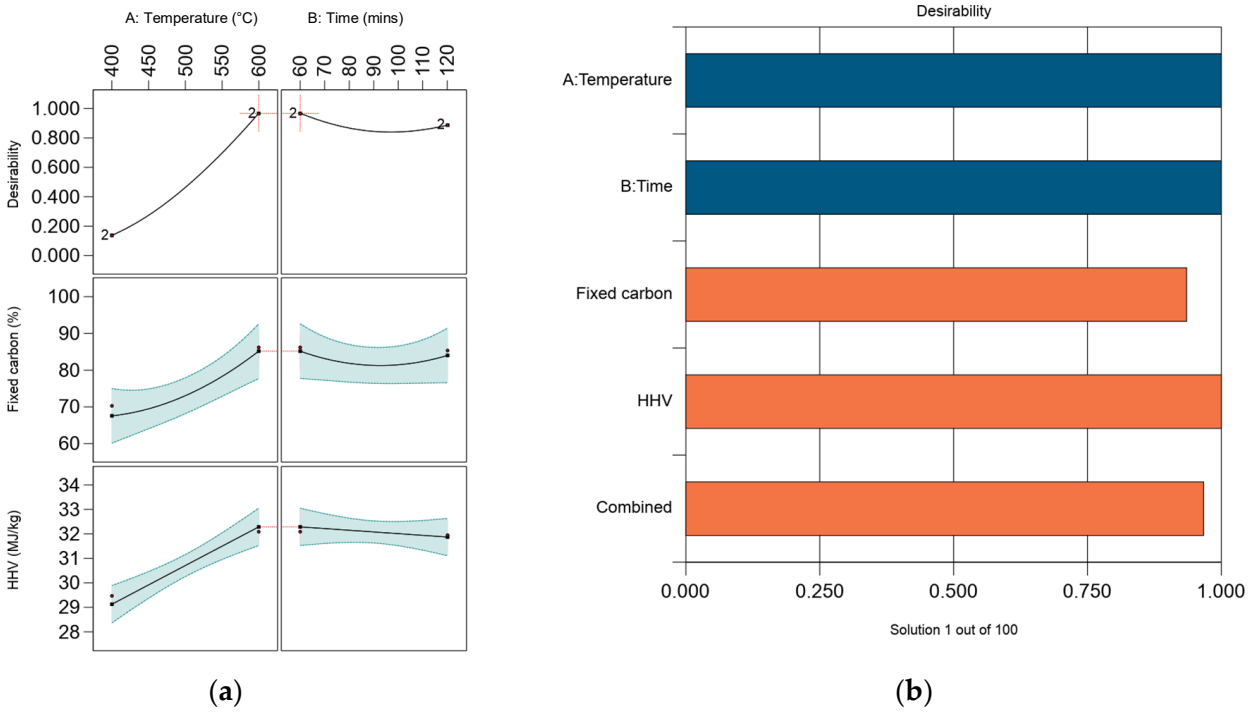

Figure 4. Profiles for the predicted values and the desirability through the desirability function method. (**a**) Red dotted lines show values after the optimization, giving the best possible outcome for fixed-carbon content and HHV of biochar, (**b**) graphical representation of the optimized conditions.

Given the statistically significant lack-of-fit associated with the HHV model, the optimization results for HHV should be considered tentative and indicative rather than definitive. Accordingly, the optimized conditions are interpreted primarily in terms of maximizing fixed-carbon content, while the associated HHVs reflect general trends within the experimental domain rather than a rigorously optimized response. Nonetheless, the experimentally obtained HHV under these conditions exceeds the minimum HHV observed in the design space (28.45 MJ/kg), supporting the suitability of high-temperature, short-residence-time pyrolysis for producing PS-derived biochar with enhanced fuel characteristics.

3.6. Characterization of Optimized Biochar

The variations in proximate composition, ultimate analysis, pH, and electrical conductivity of the PS-derived biochar produced under different pyrolysis conditions are summarized in Supplementary Table S3. Biochar produced under optimal conditions (600 °C and 60 min) exhibited markedly improved fuel quality relative to the raw PS biomass. Specifically, optimized biochar showed 58.7% reduction in moisture content, 88.0% decrease in volatile matter, 58.4% HHV increase, and 254.7% increase in fixed carbon (Table 3). Fixed carbon and volatile matter contents of the optimized biochar are comparable to those of coal, which typically range from 46 to 92 wt% and 0.5 to 50 wt%, respectively [51]. The pronounced increase in fixed carbon is attributed to extensive devolatilization during

pyrolysis, as fixed carbon represents the residual solid fraction remaining after the release of volatile components. Consequently, the solid biochar matrix became proportionally enriched in fixed carbon and ash. Pyrolysis also resulted in a slight increase in ash content with optimized biochar (4.97 ± 0.00%) compared with 1.78 ± 0.00% of raw biomass. This increase is primarily associated with the thermal transformation and concentration of inorganic constituents following the removal of organic matter, as mineral components and metallic elements remain largely non-volatile under pyrolysis conditions [22,52].

Elemental analysis provides critical insights into biochar carbon structure, stability, and fuel quality, as well as its potential for long-term carbon sequestration [28]. Optimized biochar exhibited a high C content (83.44 ± 0.53%), indicating the formation of a thermally stable carbonaceous matrix that satisfies the stability requirements of the European Biochar Certificate [9]. This value is comparable to, and slightly higher than, the C content reported for *Canarium schweinfurthii* hard-shell biochar produced at 600 °C (79.32%) [34], suggesting effective C enrichment under the applied pyrolysis conditions. The pronounced reduction in H (2.03 ± 0.04%) and O (8.57 ± 0.52%) contents reflects extensive dehydration, decarboxylation, and aromatization reactions during pyrolysis, leading to the development of a condensed aromatic structure. Consistent with this, low H:C (0.291) and O:C (0.077) molar ratios obtained for optimized biochar indicate a high degree of carbonization and enhanced thermal stability. These values fall well below the commonly accepted thresholds for poorly carbonized biochars (H:C > 0.7; O:C > 0.4), confirming the superior structural stability of optimized biochar relative to the raw biomass [53].

The use of CO_2 as a purge gas prior to heating can influence reaction pathways and thermodynamic equilibria, promoting C retention while suppressing hydrogen- and oxygen-containing functional groups [28]. This effect is evidenced by the substantial increase in C content relative to the raw biomass (50.65 ± 0.60%), consistent with previous reports of CO_2-assisted pyrolysis leading to enhanced C enrichment in biochar [28,54,55]. In the present study, CO_2 was applied only as a 30 min pre-purge and was not flowed throughout pyrolysis; therefore, any impact on the final biochar properties is expected to be minimal. Nevertheless, a more comprehensive assessment of gas-phase effects on biochar formation would benefit from comparative experiments using inert carrier gases, such as N_2, as reference conditions.

Figure 5a,b show the surface morphology of the raw biomass, while Figure 5c,d present SEM images of the optimized biochar, highlighting the structural changes induced by pyrolysis at magnifications up to 1500×. Figure 5a illustrates absence of pores in the surface of the raw feedstock. This result agreed with the structure of raw Dabai nutshells [56], where the structure was observed as rigid and packed, which is typical for lignocellulosic material. After pyrolysis, the optimized biochar exhibits a rougher surface with visible pore changes that were not apparent in the raw biomass. These qualitative morphological changes are likely from the degradation of the biomass matrix and the release of volatile matter during pyrolysis. Such porosity is advantageous, as it provides increased adsorption sites for ions and facilitates nutrient and water retention [49].

Elemental mapping (Figure 5e) confirmed the presence and spatial distribution of metals and nutrient elements. The results indicate a high C density in the optimized biochar. As summarized in Table 6, EDX analysis showed that Ca decreased from 3.06 ± 3.55% in the raw PS biomass to 1.40 ± 0.39% in the optimized biochar. Other alkali and alkaline earth metals, such as Mg and Na, as well as trace nutrient elements including N, P, and K, were also detected. These elements collectively contribute to the ash content of the biochar following pyrolysis. Detected Au (1.01 ± 0.40% in raw PS and 1.55 ± 0.20% in optimized biochar) can be attributed to the gold sputter-coating and is not intrinsic to the biochar. Trace heavy metals (Pb, Cr, Cd, Hg) were also observed. Notably, the most abundant trace

metal, Pb, became more concentrated following pyrolysis, increasing from 1.96 ± 0.86% in the raw biomass to 4.27 ± 0.68% in the optimized biochar.

Literature indicates that the bioavailability of heavy metals during biomass carbonization is strongly influenced by pyrolysis temperature, primarily due to temperature-dependent interactions between inorganic mineral phases and aromatic organic structure [18]. Elevated Pb levels may suggest caution for biochar application in food crops due to potential soil accumulation under excessive application rates [21]. It is important to note that measurements in the present study are semi-quantitative and surface-limited; therefore, any environmental or agronomic implications are considered preliminary. Further quantitative analysis would be needed to fully assess environmental or agricultural risks.

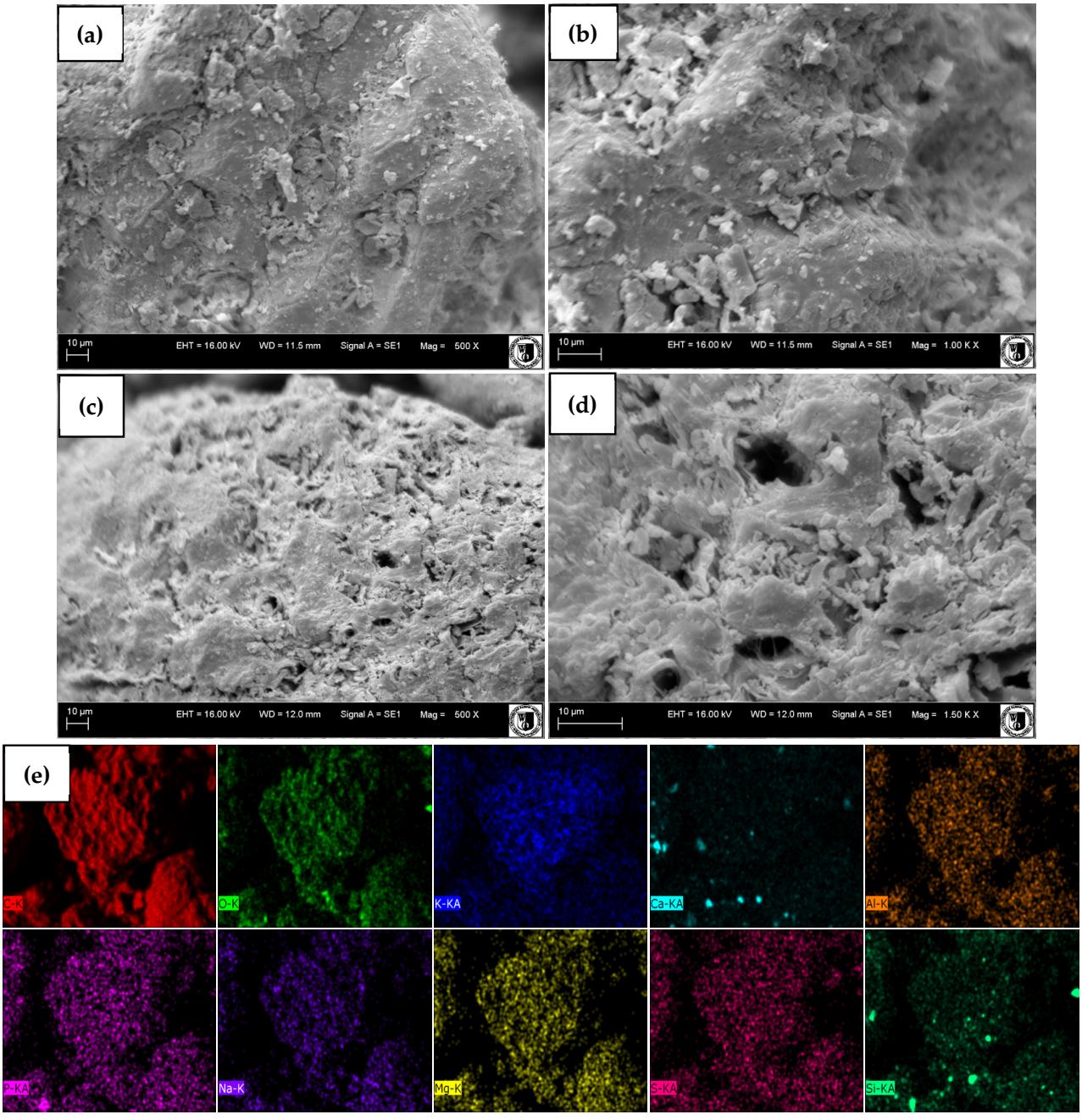

Figure 5. Scanning electron micrograph for (**a**,**b**) raw PS-biomass, (**c**,**d**) optimized biochar (600 °C, 60 min) at 500× and 1500× magnification, and (**e**) elemental mapping distribution on the optimized biochar surface at 150× magnification with 200 µm scale bar.

Table 6. Biochar elements for energy dispersive x-ray results.

Element	Series	PS-Biomass		Optimized Biochar	
		Norm. C (wt.%)	Atom. C (at.%)	Norm. C (wt.%)	Atom. C (at.%)
Magnesium	K-series	0.07 ± 0.01	0.04 ± 0.01	0.04 ± 0.04	0.02 ± 0.02
Sodium	K-series	0.39 ± 0.19	0.27 ± 0.13	0.2 ± 0.14	0.12 ± 0.09
Potassium	K-series	0.22 ± 0.05	0.09 ± 0.02	0.97 ± 0.32	0.35 ± 0.12
Calcium	K-series	3.06 ± 3.55	1.21 ± 1.44	1.40 ± 0.39	0.49 ± 0.14
Iron	K-series	0.45 ± 0.07	0.12 ± 0.03	0.42 ± 0.07	0.11 ± 0.02
Cobalt	K-series	0.23 ± 0.08	0.06 ± 0.02	0.13 ± 0.02	0.03 ± 0.00
Nickel	K-series	0.16 ± 0.06	0.04 ± 0.02	0.16 ± 0.02	0.04 ± 0.00
Copper	K-series	0.20 ±0.05	0.05 ± 0.02	0.2 ± 0.04	0.05 ± 0.01
Sulfur	K-series	0 ± 0.00	0 ± 0.00	0.01 ± 0.01	0.003 ± 0.01
Oxygen	K-series	51.48 ± 1.07	49.42 ± 1.39	16.46 ± 1.46	14.46 ± 1.30
Chlorine	K-series	0.22 ± 0.19	0.10 ± 0.08	0.08 ± 0.03	0.03 ± 0.02
Fluorine	K-series	1.12 ± 0.80	0.90 ± 0.63	0.45 ± 0.20	0.33 ± 0.14
Carbon	K-series	36.58 ± 3.14	46.70 ± 2.18	70.92 ± 1.86	83 ± 1.55
Silicon	K-series	0.80 ± 0.33	0.43 ± 0.17	0.59 ± 0.23	0.30 ± 0.12
Phosphorus	K-series	0.15 ± 0.13	0.07 ± 0.06	0.06 ± 0.04	0.03 ± 0.02
Zinc	K-series	0.13 ± 0.03	0.03 ± 0.01	0.19 ± 0.03	0.04 ± 0.01
Lead	L-series	1.96 ± 0.86	0.15 ± 0.07	4.27 ± 0.68	0.29 ± 0.05
Cadmium	L-series	0.49 ± 0.41	0.07 ± 0.05	0.21 ± 0.08	0.02 ± 0.01
Chromium	K-series	0.23 ± 0.09	0.06 ± 0.03	0.17 ± 0.03	0.05 ± 0.01
Manganese	K-series	0.16 ± 0.09	0.04 ± 0.03	0.10 ± 0.04	0.03 ± 0.01
Arsenic	K-series	0 ± 0.00	0 ± 0.00	0 ± 0.00	0 ± 0.00
Gold	L-series	1.01 ± 0.40	0.08 ± 0.04	1.55 ± 0.20	0.11 ± 0.02
Mercury	L-series	0.85 ± 0.42	0.06 ± 0.04	1.39 ± 0.34	0.10 ± 0.03
Molybdenum	L-series	0.02 ± 0.03	0.003 ± 0.01	0.03 ± 0.04	0.003 ± 0.01
Total:		100	100	100	100

An increased pH value is a direct result of an increasing degree of carbonization [15]. The pH of optimized biochar was found to be 9.45 ± 0.04. This alkalinity arises from the accumulation of non-volatile inorganic constituents and nutrient elements remaining after pyrolysis. Functional groups removed during pyrolysis are predominantly acidic in nature, including carboxyl, hydroxyl, and formyl groups; consequently, the remaining solid becomes more basic [15]. The optimized biochar exhibited an electrical conductivity of 0.30 mS/cm, suggesting enhanced ionic mobility. Notably, the pH and electrical conductivity values obtained under optimal conditions were approximately twofold higher than those of the raw biomass (pH = 5.34; electrical conductivity = 0.15 mS/cm), as shown in Table 3.

The thermal behavior of the optimized biochar, compared with raw PS biomass, is presented in Figure 6. It is important to note that TGA was conducted under nitrogen rather than CO_2, as previous studies indicate that the atmosphere has minimal effect on decomposition onset and end temperatures [28]. The heating rate of 15 °C/min was maintained to closely mimic the conditions of pyrolysis. PS biomass exhibited an initial decomposition temperature of 107.75 °C, marking the onset of thermal degradation following moisture evaporation [25]. The optimized biochar also displayed minimal weight loss at 110.06 °C, attributable to the removal of physically adsorbed moisture, indicating its low residual water content. PS biomass underwent a major weight loss of 69.20% between 269.88 and 365.75 °C, corresponding to the decomposition of cellulose and hemicellulose [57]. The optimized biochar showed remarkable thermal stability across the entire high-temperature range, with only a gradual mass loss of approximately 0.87% between 667.96 and 773.35 °C, likely due to the release of residual volatiles. The residual mass fraction of optimized biochar was 90.4% of its initial weight, compared with 23.24% for raw PS biomass, demonstrating effective volatile removal and the

formation of a thermally stable, carbon-rich structure. The flat thermogram (TG) profile of the optimized biochar indicates an enhanced thermal stability suitable for solid fuel use.

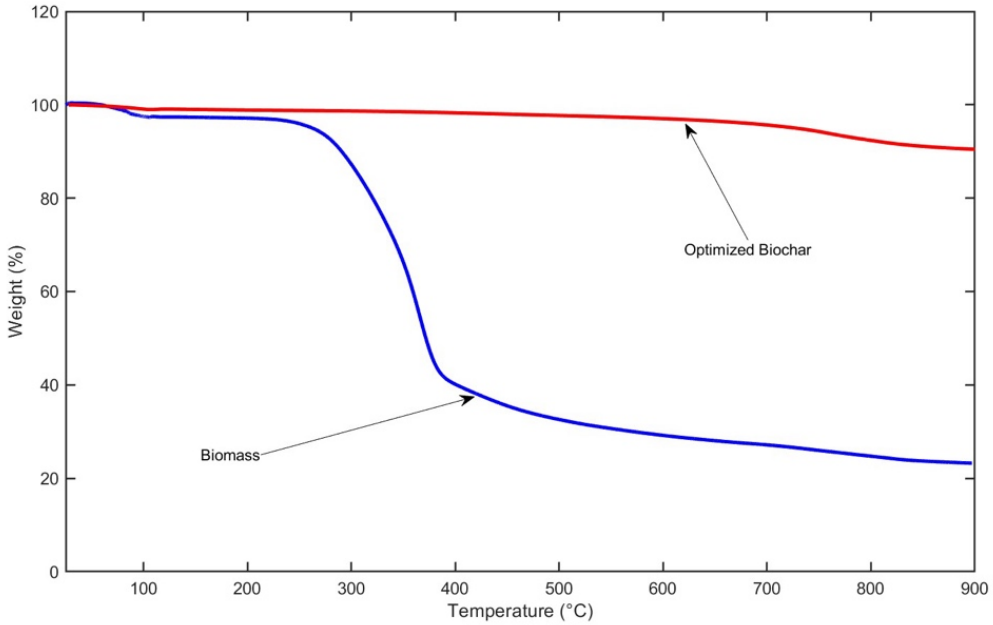

Figure 6. TG curves of raw PS biomass and optimized biochar under 600 °C for 60 min.

4. Conclusions

The RSM based on CCD was employed to optimize the pyrolysis conditions for producing biochar from PS, a regionally significant feedstock in the Bicol Region, Philippines, with fixed-carbon content and HHV as the primary fuel quality indicators. Based on the results, PS-derived biochar demonstrated suitability as a solid fuel. Pyrolysis temperature exerted the most pronounced influence on both fixed-carbon content and HHV. A maximum fixed-carbon content of 86.15% and an HHV of 32.10 MJ/kg were achieved at the optimal pyrolysis conditions of 600 °C and a residence time of 60 min. The HHV of the optimized PS-derived biochar is comparable to that of coal, which typically ranges from 25 to 35 MJ/kg [51]. However, due to the statistically significant lack-of-fit associated with the HHV model, the optimization result for HHV is regarded as indicative rather than definitive and represents a trend-based outcome rather than a precise predictive optimum.

Under the optimal conditions, the experimentally obtained mass yield, energy densification ratio, and energy yield were 29.11%, 158.4%, and 46.1%, respectively. Thermogravimetric analysis confirmed that the optimized pyrolysis conditions effectively transformed the raw biomass into a thermally stable biochar, characterized by reduced volatile matter (8.88%), low ash content (4.97%), and low atomic ratios (H:C = 0.291; O:C = 0.077). Alkali and alkaline earth metals and trace nutrients were detected on the surface of the optimized biochar, with Pb being the predominant heavy metal. As the elemental distribution analysis is semi-quantitative and surface-limited, further quantitative assessments are required to evaluate potential environmental or agricultural risks.

The improved thermal stability of the optimized PS-derived biochar indicates its potential for fuel-related applications, soil amendment due to its alkaline nature [58] and long-term carbon sequestration [58,59]. However, this study has several limitations, including the restriction of the optimization to only two process variables—pyrolysis temperature and residence time. The inclusion of additional variables or more complex models could improve HHV prediction and could be explored in future studies, together with the direct performance testing of the biochar as a fuel. Consequently, the optimized conditions re-

ported herein should be interpreted as feedstock-specific. Further validation using other biomass residues is required to assess the broader applicability of the proposed RSM-based optimization framework. In addition, the high volatile-matter content of the raw biomass suggests favorable characteristics for thermochemical conversion pathways, particularly bio-oil production, which merits further investigation.

Supplementary Materials: The following supporting information can be downloaded at: https://www.mdpi.com/article/10.3390/biomass6020022/s1, Table S1: Biochar production performance; Table S2: Solutions from numerical optimization; and Table S3: Physicochemical composition, ultimate analysis, pH and electrical conductivity of different biochars.

Author Contributions: Conceptualization, A.M., W.M., K.P. and J.L.; methodology, A.M., M.V. and J.L.; software, A.M. and K.P.; validation, A.M., J.L. and K.P.; formal analysis, A.M., J.L., A.B. (Antonio Barroga), M.D. and W.M.; investigation, A.M., M.V. and J.L.; resources, A.M., A.B. (Antonio Barroga), A.B. (Andrzej Białowiec) and M.V.; data curation, A.M., K.P., M.V. and J.L.; writing—original draft preparation, A.M.; writing—review and editing, A.M., A.B. (Antonio Barroga), W.M., A.B. (Andrzej Białowiec), M.D. and J.L.; visualization, A.M. and K.P.; supervision, A.B. (Andrzej Białowiec), J.L. and M.V.; project administration, A.B. (Andrzej Białowiec), J.L. and M.V.; funding acquisition, W.M. and A.B. (Andrzej Białowiec). All authors have read and agreed to the published version of the manuscript.

Funding: This research was funded by the Department of Science and Technology–Engineering Research and Development for Technology (DOST-ERDT).

Data Availability Statement: The data presented in this study are contained within the article and Supplementary Materials.

Acknowledgments: This work was implemented at the Department of Applied Bioeconomy, Wrocław University of Environmental and Life Sciences, Poland, with the support of the Department of Science and Technology—Engineering Research and Development for Technology (ERDT) and Central Luzon State University (CLSU), Philippines. The authors acknowledge the Albay Provincial Agricultural Office (APAO) Pili Processing Facility in Camalig, Albay, Philippines, for providing the Pili nutshell samples used in this study. During the preparation of this manuscript, the authors used OpenAI's ChatGPT-4o (December 2025 version) to assist in refining technical phrasing and grammar. MATLAB (R2024a) code snippets for data analysis and figure preparation. All outputs were reviewed, edited, and validated by the author, who assumes full responsibility for the final content of this publication.

Conflicts of Interest: The authors declare no conflicts of interest.

References

1. Rashid, N.A.H.A.; Shamsudin, R.; Arifin, S.H.; Abdullah, W.N.Z.Z. Morphological and quality characteristics of genus of *Canarium* L.: A review. *IOP Conf. Ser. Earth Environ. Sci.* **2021**, *733*, 012015. [CrossRef]
2. Alguzar, C.V.; Rey, J.D. *Canarium ovatum* Engl.: The Next Wonder Tree of the Philippines. *Diliman Rev.* **2022**, *66*, 97–116.
3. Millena, C.G.; Baloloy, K.A.V.; Doma, N.G.; Hernan, P.B. Effect of Maturity on Physicochemical and Fatty Acid Profile of Philippine Pili (*Canarium ovatum* Engl.). *Philipp. J. Sci.* **2023**, *152*, 159–171. [CrossRef]
4. Philippine Statistics Authority. *Supply Utilization Accounts (SUA) of Selected Agriculture and Fishery Commodities*; Philippine Statistics Authority: Quezon City, Philippines, 2023.
5. Gallegos, R.K.B.; Suministrado, D.; Amongo, R.M.C.; Madlangbayan, M. Some Physical and Mechanical Properties of Pili (*Canarium ovatum* Engl. cv. Katutubo) Nut as a Function of Nut Moisture Content. *Philipp. Agric. Sci.* **2013**, *96*, 66–74.
6. Millena, C.G.; Sagum, R.S. Philippine Pili (*Canarium ovatum*, Engl.) varieties as source of essential minerals and trace elements in human nutrition. *J. Food Compos. Anal.* **2018**, *69*, 53–61. [CrossRef]
7. Dumandan, N.G.; Kagaoan, A.C.T.; Acda, R.D.P.; Tumambing, C.R.; Pham, L.J. Extraction, Profiling, and Characterization of Phytosterols and Triterpenoids from Pili (*Canarium ovatum* Engl.) Pulp Oil Exhibiting Antioxidant and Antibacterial Properties. *Biochem. Res. Int.* **2022**, *2022*, 6604984. [CrossRef] [PubMed]

8. Arya, G.; Kumar, N.; Gupta, N.; Kumar, A.; Nimesh, S. Antibacterial potential of silver nanoparticles biosynthesised using *Canarium ovatum* leaves extract. *IET Nanobiotechnol.* **2017**, *11*, 506–511. [CrossRef]
9. EBC. European Biochar Certificate—Guidelines for a Sustainable Production of Biochar. 2024. Available online: http://www.european-biochar.org/media/doc/2/version_en_10_4.pdf (accessed on 30 January 2025).
10. Afshar, M.; Mofatteh, S. Biochar for a sustainable future: Environmentally friendly production and diverse applications. *Results Eng.* **2024**, *23*, 102433. [CrossRef]
11. Han, Y.; Luo, Y.; Zhang, L.; Lu, X.; Luo, X.; Wu, X.; Zan, F. Deciphering the mechanistic insight into modified biochar for distinct anaerobic digestion processes: Surface functional groups and electron-transmitting capabilities. *J. Environ. Chem. Eng.* **2025**, *13*, 115581. [CrossRef]
12. He, D.; Luo, Y.; Zhu, B. Feedstock and pyrolysis temperature influence biochar properties and its interactions with soil substances: Insights from a DFT calculation. *Sci. Total Environ.* **2024**, *922*, 171259. [CrossRef]
13. Pap, S.; Gaffney, P.P.J.; Zhao, Q.; Klein, D.; Li, Y.; Kirk, C.; Taggart, M.A. Optimising production of a biochar made from conifer brash and investigation of its potential for phosphate and ammonia removal. *Ind. Crops Prod.* **2022**, *185*, 115165. [CrossRef]
14. Luo, Q.; Deng, Y.; Li, Y.; He, Q.; Wu, H.; Fang, X. Effects of pyrolysis temperatures on the structural properties of straw biochar and its adsorption of tris-(1-chloro-2-propyl) phosphate. *Sci. Rep.* **2024**, *14*, 25711. [CrossRef]
15. Weber, K.; Quicker, P. Properties of biochar. *Fuel* **2018**, *217*, 240–261. [CrossRef]
16. Wood, R.; Mašek, O.; Erastova, V. Developing a molecular-level understanding of biochar materials using public characterization data. *Cell Rep. Phys. Sci.* **2024**, *5*, 102036. [CrossRef]
17. Xiao, X.; Chen, Z.; Chen, B. H/C atomic ratio as a smart linkage between pyrolytic temperatures, aromatic clusters and sorption properties of biochars derived from diverse precursory materials. *Sci. Rep.* **2016**, *6*, 22644. [CrossRef]
18. Shi, W.; Lian, W.; Tian, S.; Gong, X.; Yu, Q.; Guo, Z.; Zhang, X.; Ma, B.; Bian, R.; Zheng, J.; et al. A review of agronomic and environmental properties of inorganic compounds in biochars. *Curr. Res. Environ. Sustain.* **2023**, *5*, 100226. [CrossRef]
19. Rajkovich, S.; Enders, A.; Hanley, K.; Hyland, C.; Zimmerman, A.R.; Lehmann, J. Corn growth and nitrogen nutrition after additions of biochars with varying properties to a temperate soil. *Biol. Fertil. Soils* **2012**, *48*, 271–284. [CrossRef]
20. Deru, J.G.C.; Hoekstra, N.; van Agtmaal, M.; Bloem, J.; de Goede, R.; Brussaard, L.; van Eekeren, N. Effects of Ca:Mg ratio and pH on soil chemical, physical and microbiological properties and grass N yield in drained peat soil. *N. Z. J. Agric. Res.* **2023**, *66*, 61–82. [CrossRef]
21. Roman, A.; Bucura, F.; Botoran, O.R.; Radu, G.-L.; Niculescu, V.-C.; Soare, A.; Ion-Ebrasu, D.; Vagner, I.; Dunca, E.-C.; Șandru, C.; et al. Thermochemical processing of agricultural waste into biochar with potential application for coal mining degraded soils. *Results Eng.* **2025**, *26*, 105497. [CrossRef]
22. Mohit, A.; Remya, N. Optimization of biochar production from greywater grown polyculture microalgae using microwave pyrolysis. *Bioresour. Technol.* **2023**, *388*, 129666. [CrossRef]
23. Egbosiuba, T.C. Biochar and bio-oil fuel properties from nickel nanoparticles assisted pyrolysis of cassava peel. *Heliyon* **2022**, *8*, e10114. [CrossRef] [PubMed]
24. Talib, N.A.A.; Salam, F.; Yusof, N.A.; Alang Ahmad, S.A.; Sulaiman, Y. Optimization of peak current of poly(3,4-ethylenedioxythiophene)/multi-walled carbon nanotube using response surface methodology/central composite design. *RSC Adv.* **2017**, *7*, 11101–11110. [CrossRef]
25. Papa, K.; Lavarias, J.; Denson, M.; Paragas, D.; Tanquilut, M.R.; Morico, A. Characterization, Kinetic Studies, and Thermodynamic Analysis of Pili (*Canarium ovatum* Engl.) Nutshell for Assessing Its Biofuel Potential and Bioenergy Applications. *Fuels* **2026**, *7*, 2. [CrossRef]
26. *PN-EN ISO 18134-2:2017-03E*; In Solid Biofuels. Determination of Moisture Content—Oven Dry Method—Part 2: Total Moisture—Simplified Method. European Committee for Standardization: Brussels, Belgium, 2017.
27. Świechowski, K.; Rosik, J.; Bednik, M.; Szatkowska, B.; Tomczak-Wandzel, R.; Stegenta-Dąbrowska, S. Heracleum sosnowskyi pyrolysis—Energy and environmental aspects of biochar utilization. *Bioresour. Technol.* **2024**, *408*, 131169. [CrossRef]
28. Premchand, P.; Demichelis, F.; Chiaramonti, D.; Bensaid, S.; Fino, D. Study on the effects of carbon dioxide atmosphere on the production of biochar derived from slow pyrolysis of organic agro-urban waste. *Waste Manag.* **2023**, *172*, 308–319. [CrossRef]
29. Stefanów, J.; Sobieraj, K.; Hejna, M.; Pawęska, K.; Świechowski, K. Fuel Characteristics and Phytotoxicity Assay of Biochar Derived from Rose Pruning Waste. *Materials* **2024**, *17*, 1895. [CrossRef]
30. Torquato, L.D.M.; Crnkovic, P.M.; Ribeiro, C.A.; Crespi, M.S. New approach for proximate analysis by thermogravimetry using CO_2 atmosphere: Validation and application to different biomasses. *J. Therm. Anal. Calorim.* **2017**, *128*, 1–14. [CrossRef]
31. *PN-EN ISO 16948: 2015-07*; Solid Biofuels—Determination of Total Carbon, Hydrogen and Nitrogen Content. European Committee for Standardization: Brussels, Belgium, 2015.
32. *PN-EN ISO 18125:2017-07*; Solid Biofuels—Determination of Calorific Value. European Committee for Standardization: Brussels, Belgium, 2017.
33. Rohit Kaushal, R. Experimental investigation of the gasification characteristics of coconut husk and walnut shell blend in an open core downdraft gasifier. *Energy Convers. Manag.* **2025**, *345*, 120390. [CrossRef]

34. Garba, K.; Mohammed, I.Y.; Isa, Y.M.; Abubakar, L.G.; Abakr, Y.A.; Hameed, B.H. Pyrolysis of *Canarium schweinfurthii* hard-shell: Thermochemical characterisation and pyrolytic kinetics studies. *Heliyon* **2023**, *9*, e13234. [CrossRef]
35. Racero-Galaraga, D.; Rhenals-Julio, J.D.; Sofan-German, S.; Mendoza, J.M.; Bula-Silvera, A. Proximate analysis in biomass: Standards, applications and key characteristics. *Results Chem.* **2024**, *12*, 101886. [CrossRef]
36. Rambhatla, N.; Panicker, T.F.; Mishra, R.K.; Manjeshwar, S.K.; Sharma, A. Biomass pyrolysis for biochar production: Study of kinetics parameters and effect of temperature on biochar yield and its physicochemical properties. *Results Eng.* **2025**, *25*, 103679. [CrossRef]
37. Borges, A.D.S.; Cardoso, M.; Oliveira, M. Thermochemical evaluation of biochars properties from Portuguese agro-forestry residues for solid fuel applications. *Sci. Rep.* **2025**, *16*, 1120. [CrossRef] [PubMed]
38. Rangabhashiyam, S.; Balasubramanian, P. The potential of lignocellulosic biomass precursors for biochar production: Performance, mechanism and wastewater application—A review. *Ind. Crops Prod.* **2019**, *128*, 405–423. [CrossRef]
39. Hejna, M.; Świechowski, K.; Białowiec, A. Study on the Effect of Hydrothermal Carbonization Parameters on Fuel Properties of Sewage Sludge Hydrochar. *Materials* **2023**, *16*, 6903. [CrossRef] [PubMed]
40. Anshariah Imran, A.M.; Widodo, S.; Irvan, U.R. Correlation of fixed carbon content and calorific value of South Sulawesi Coal, Indonesia. *IOP Conf. Ser. Earth Environ. Sci.* **2020**, *473*, 012106. [CrossRef]
41. Ruiz-Aguilar, G.M.L.; Martínez-Martínez, J.H.; Costilla-Salazar, R.; Camarena-Martínez, S. Using Central Composite Design to Improve Methane Production from Anaerobic Digestion of Tomato Plant Waste. *Energies* **2023**, *16*, 5412. [CrossRef]
42. Onu, C.E.; Nweke, C.N.; Nwabanne, J.T. Modeling of thermo-chemical pretreatment of yam peel substrate for biogas energy production: RSM, ANN, and ANFIS comparative approach. *Appl. Surf. Sci. Adv.* **2022**, *11*, 100299. [CrossRef]
43. Ibitoye, S.E.; Loha, C.; Mahamood, R.M.; Olayemi, O.A.; Alam, M.; Jen, T.-C.; Abdullahi, M.J.; Akinlabi, E.T. Optimization of Rice Straw Properties via Torrefaction for Solid Fuel Applications. *Bioenergy Res.* **2025**, *18*, 95. [CrossRef]
44. Ghelich, R.; Jahannama, M.R.; Abdizadeh, H.; Torknik, F.S.; Vaezi, M.R. Central composite design (CCD)-Response surface methodology (RSM) of effective electrospinning parameters on PVP-B-Hf hybrid nanofibrous composites for synthesis of HfB_2-based composite nanofibers. *Compos. B Eng.* **2019**, *166*, 527–541. [CrossRef]
45. Wakatuntu, J.; Olupot, P.W.; Jjagwe, J.; Menya, E.; Okure, M. Optimization of pyrolysis conditions for production of rice husk-based bio-oil as an energy carrier. *Results Eng.* **2023**, *17*, 100947. [CrossRef]
46. Ramani, B.; Anjum, A.; Bramer, E.; Dierkes, W.; Blume, A.; Brem, G. A comprehensive study on the effect of the pyrolysis temperature on the products of the flash pyrolysis of waste tires. *J. Environ. Chem. Eng.* **2025**, *13*, 115468. [CrossRef]
47. Singh, C.; Goyal, R.; Saluja, N. Optimization of pyrolysis process parameters for optimal high heating value of biochar produced from rice straw. *Biofuels* **2025**, *16*, 706–716. [CrossRef]
48. Jamaluddin, M.A.; Ismail, K.; Mohd Ishak, M.A.; Ab Ghani, Z.; Abdullah, M.F.; Safian, M.T.-U.; Idris, S.S.; Tahiruddin, S.; Yunus, M.F.M.; Hakimi, N.I.N.M. Microwave-assisted pyrolysis of palm kernel shell: Optimization using response surface methodology (RSM). *Renew. Energy* **2013**, *55*, 357–365. [CrossRef]
49. Rout, T.; Pradhan, D.; Singh, R.K.; Kumari, N. Exhaustive study of products obtained from coconut shell pyrolysis. *J. Environ. Chem. Eng.* **2016**, *4*, 3696–3705. [CrossRef]
50. Bhushan, D.; Tomar, K.; Mondal, P. Multi-parameter optimization and predictive modeling of pyrolysis of walnut shells in fixed bed reactor using response surface methodology and machine learning algorithms. *J. Anal. Appl. Pyrolysis* **2025**, *192*, 107242. [CrossRef]
51. Chen, W.H.; Peng, J.; Bi, X.T. A state-of-the-art review of biomass torrefaction, densification and applications. *Renew. Sustain. Energy Rev.* **2015**, *44*, 847–866. [CrossRef]
52. Pradhan, S.; Shahbaz, M.; Abdelaal, A.; Al-Ansari, T.; Mackey, H.R.; McKay, G. Optimization of process and properties of biochar from cabbage waste by response surface methodology. *Biomass Convers. Biorefinery* **2022**, *12*, 5479–5491. [CrossRef]
53. Amalina, F.; Razak, A.S.A.; Krishnan, S.; Sulaiman, H.; Zularisam, A.W.; Nasrullah, M. Biochar production techniques utilizing biomass waste-derived materials and environmental applications—A review. *J. Hazard. Mater. Adv.* **2022**, *7*, 100134. [CrossRef]
54. Lee, J.; Yang, X.; Song, H.; Ok, Y.S.; Kwon, E.E. Effects of carbon dioxide on pyrolysis of peat. *Energy* **2017**, *120*, 929–936. [CrossRef]
55. Yi, Z.; Li, C.; Zhang, L.; Zhang, S.; Gao, W.; Wang, S.; Li, B.; Hu, X. Impacts of CO_2 atmosphere on property of the biochar from pyrolysis of lignin. *J. Anal. Appl. Pyrolysis* **2022**, *167*, 105689. [CrossRef]
56. Bin Mohd Khairulzaim, A.A.; Rahman, M.R.; Roslan, L.; Bin Bakri, M.K.; Khan, A.; Matin, M.M. Analysis of Char Prepared by Pyrolysis of Dabai (*Canarium odontophyllum*) Nutshells as a Potential Precursor of Biocarbon Used for Wastewater Treatment. *Bioresources* **2021**, *16*, 5036–5046. [CrossRef]
57. Menya, E.; Olupot, P.W.; Storz, H.; Lubwama, M.; Kiros, Y.; John, M.J. Optimization of pyrolysis conditions for char production from rice husks and its characterization as a precursor for production of activated carbon. *Biomass Convers. Biorefinery* **2020**, *10*, 57–72. [CrossRef]

58. Chen, L.; Al-Dhabi, N.A.; Ai, W.; Sun, S.; Peng, Y.; Gao, C.; Zhuo, Y.; Tang, W.; Zhou, Y.; Sun, C. Impact of low-temperature pyrolysis on ash and physicochemical properties of straw biochar: Multivariate analysis and implications for agricultural and environmental use. *Ind. Crops Prod.* **2025**, *224*, 120431. [CrossRef]
59. Tomczyk, A.; Sokołowska, Z.; Boguta, P. Biochar physicochemical properties: Pyrolysis temperature and feedstock kind effects. *Rev. Environ. Sci. Biotechnol.* **2020**, *19*, 191–215. [CrossRef]

Disclaimer/Publisher's Note: The statements, opinions and data contained in all publications are solely those of the individual author(s) and contributor(s) and not of MDPI and/or the editor(s). MDPI and/or the editor(s) disclaim responsibility for any injury to people or property resulting from any ideas, methods, instructions or products referred to in the content.